Pergamon

Solar Energy, Vol. 53, No. 1, pp. 57–71, 1994

0038-092X/94 $6.00 + .00

0038-092X(94)E0009-2

ANALYSIS OF MONTHLY AVERAGE ATMOSPHERIC PRECIPITABLE WATER AND TURBIDITY IN CANADA AND NORTHERN UNITED STATES

CHRISTIAN GUEYMARD*
Florida Solar Energy Center, 300 State Road 401, Cape Canaveral, FL 32920, U.S.A.

Abstract—Atmospheric turbidity and precipitable water data are necessary as inputs to solar radiation or daylight availability models, and to daylighting simulation programs. A new model is presented to obtain precipitable water from long-term averages of temperature and humidity. Precipitable water data derived from this model are tabulated for some Canadian and northern U.S. sites. A discussion on the available turbidity data is presented. An analysis of the datasets from the WMO turbidity network is detailed. The effect of volcanic eruptions is discussed, as well as the possible comparisons with indirect determinations of turbidity from radiation data. A tabulation of the monthly average turbidity coefficients for ten Canadian stations and seven northern U.S. stations of the WMO network is presented.

1. INTRODUCTION

Precipitable water and turbidity are two important atmospheric parameters that are needed when using physical or empirical models to predict solar radiation. These parameters may also be needed to evaluate the illuminance and distribution of luminance in the sky [Navvab (1984)] and to perform daylighting calculations with building simulation programs such as DOE-2 [Winkelmann (1983)]. For example, the DOE-2 manual [Simulation Research Group (1989), Winkelmann (1983)] lists the monthly average values of precipitable water for 63 U.S. locations and of turbidity for 40 U.S. locations. Clearly, this dataset is too limited for a worldwide use of such calculation tools. Moreover, the accuracy of some DOE-2 turbidity data may be questionable [Gueymard (1993b)], thus leading to possible inaccuracies in the balance between direct and diffuse irradiance or illuminance. The monitoring of atmospheric turbidity is also of paramount importance when assessing the impact of anthropogenic aerosols on the climate of cities, or when estimating their cooling effect in the present climatic trend of global warming.

Precipitable water can be calculated from radiosonde pressure, humidity, and temperature data. However, no monthly average values have been tabulated from such measurements for Canada, whereas these are available at a number of U.S. sites, at least for various periods before 1972 [Garrison and Adler (1990), Lott (1976), Reitan (1960), Shands (1949)]. Using a new correlation relating the water vapor scale height to temperature and relative humidity, monthly average values of precipitable water are evaluated for some selected sites where the basic data are available.

Observed atmospheric turbidity data are particularly scarce in North America, and even more in the rest of the world. This article presents a critical review of available turbidity data that have been derived from radiation data at a few Canadian sites. Furthermore, an analysis of the observed aerosol optical thickness and turbidity coefficients at a number of Canadian and northern U.S. sites is proposed. The correspondence between the different turbidity coefficients will also be discussed.

2. PRECIPITABLE WATER

2.1 *Existing data*

Different datasets present the monthly average total precipitable water, w, for the U.S.A. Shands (1949) reported monthly average data from 4 years for 29 stations. This dataset was then extended by Reitan (1960) to 52 stations, most of them with 11 years of data. This was again updated by Lott (1976), who presented detailed data for 103 stations with measuring periods of up to 27 years depending on availability of data. A recent study [Garrison and Adler (1990)] examines all these existing data and present them in a more convenient form (but for 82 stations only), with only minor adjustments. Finally, a new dataset of hourly meteorological and radiation data has been developed for the period 1961–90 for 239 U.S. locations [NREL (1992)]. Monthly precipitable water statistics were calculated for this period and tabulated [NREL (1992)]. However, actual measured data were available at only 84 sites up to 1988, so that an empirical model was used to derive the hourly data at most sites and to fill in the data gaps at the measuring sites [Myers and Maxwell (1992)].

Very few monthly average precipitable water data are available in Canada for specific sites. Polavarapu (1978) computed monthly average data of precipitable water at Goose, Newfoundland, from upper air soundings, for the period 1969–71. Hay (1971) presented a map of precipitable water contours for each month,

* ISES member.

based on simple station-wise linear regressions between w and the surface vapor pressure, e_v. Although 34 Canadian stations were used in Hay's study, most of the upper-air stations operated by the Atmospheric Environment Service are located at high latitudes, so that the extrapolation to southern locations may be inaccurate.

2.2 *Analysis*

Reitan (1963) showed that w is, in first approximation, proportional to the surface water vapor density, ρ_v. From his analysis, it can be shown that, for ρ_v expressed in g m^{-3} and w in ppw-cm (or g cm^{-2}):

$$w = 0.1 H_v \rho_v \qquad (1)$$

where H_v is the apparent water vapor scale height (in kilometers) and the coefficient 0.1 is necessary to reconcile units. Water vapor density is a function of relative humidity, R_H, temperature, T (expressed in K), and saturation water vapor pressure, e_s (a function of temperature, expressed here in mb) [Gueymard (1993a)]. Assimilating water vapor to a perfect gas, ρ_v is obtained by [see, e.g., Garrison and Adler (1990)]:

$$\rho_v = 216.7\, R_H e_s / T \qquad (2)$$

Reitan (1963) based his analysis on the fact that ρ_v was decreasing exponentially with altitude, z, according to:

$$\rho_v(z)/\rho_v(0) = \exp(-\gamma z) \qquad (3)$$

where the decay coefficient, $\gamma = 1/H_v$, was assumed to be 0.44 km^{-1} (i.e., $H_v = 2.273$ km). Total precipitable water was obtained by integrating eqn (3) along the vertical profile, leading to eqn (1) for a sea-level site. Leckner (1978) derived an equivalent scale height (2.278 km) using eqn (3) with $\gamma = 0.439$ km^{-1}.

A closer look at humidity profiles corresponding to reference atmospheres [Anderson *et al.* (1986), Anon. (1966)] shows that the assumption of a constant decay rate, as expressed by eqn (3), is not always valid. This is apparent in Fig. 1, where profiles of $\rho_v(z)/\rho_v(0)$ are shown on a logarithmic scale for altitudes from 0 to 4

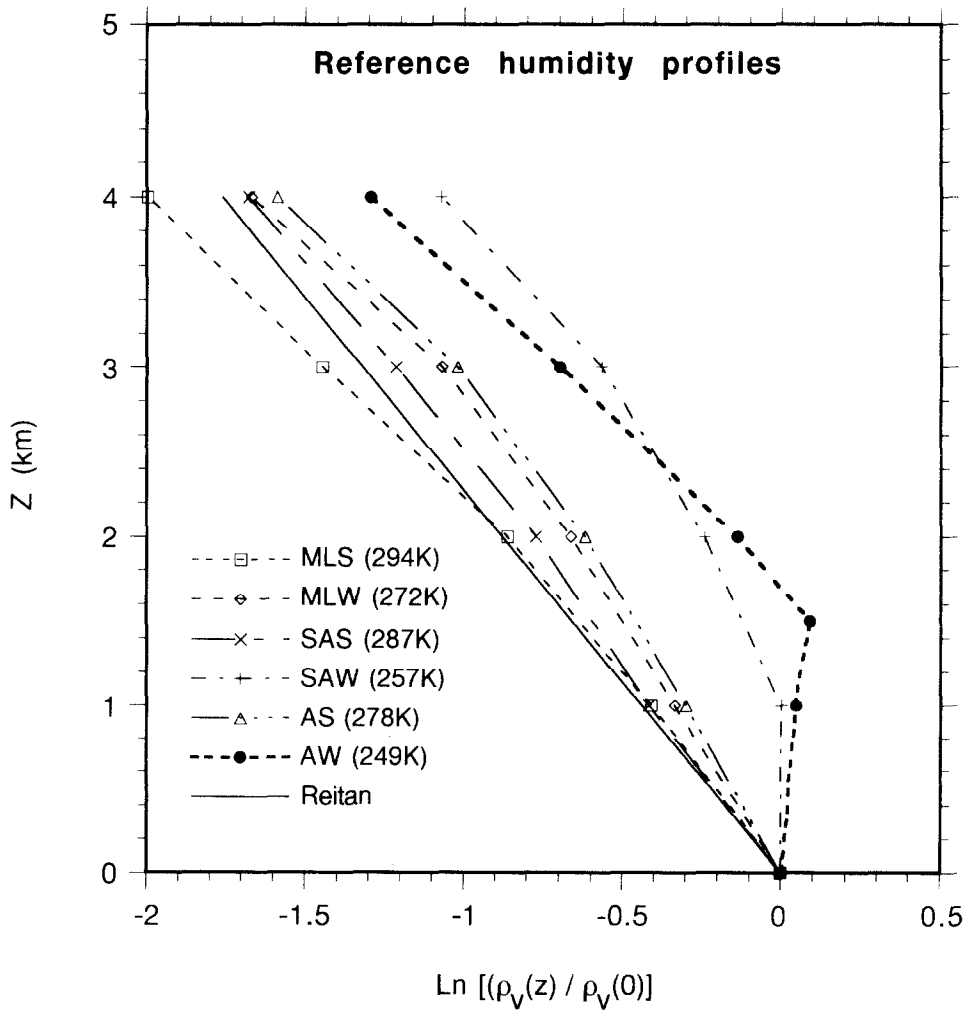

Fig. 1. Normalized vertical humidity profiles according to Reitan's empirical model, and for reference atmospheres (MLS: Mid Latitude Summer; MLW: Mid Latitude Winter; SAS: Sub Arctic Summer; SAW: Sub Arctic Winter; AS: Arctic Summer; AW: Arctic Winter). Surface-level temperatures are indicated inside brackets for each reference atmosphere.

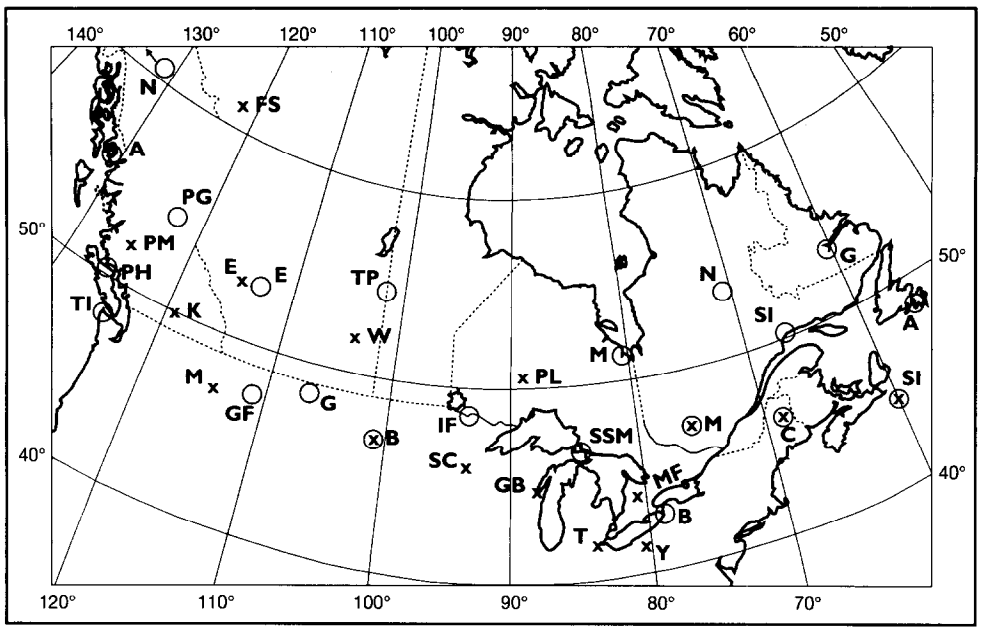

Fig. 2. Location of the primary upper air (circles) and turbidity (crosses) stations used in this study, with their initials.

km (where about 90% of the total atmospheric water vapor is concentrated) and for six reference atmospheres, chosen to match the latitudinal range of this study. Clearly, Reitan's decay coefficient agrees rather well to the MidLatitude Summer and SubArctic Summer profiles, which correspond to surface temperatures of 21°C and 14°C, respectively. However, departure from the idealized Reitan profile is apparent for colder atmospheres. The lower the surface temperature, the more frequent become inversion layers, thus preventing the proper mixing of humidity in the first few kilometers above the surface. The presence of an inversion layer necessarily corresponds to an increase of the apparent water vapor scale height with decreasing temperature. The departure from Reitan's profile is particularly pronounced with the SubArctic Winter and Arctic Winter atmospheres, whose surface temperatures are −16°C and −24°C, respectively. Such cold temperatures are typical not only of high-latitude sites in Alaska and Canada, but also of continental, mid-

Table 1. Upper air stations used in the present study

Station	Latitude	Longitude	Alt. (m)	Period
Canada				
Argentia, Nfld.	47°18 N	54°00 W	19	1961–70
Edmonton, Alta.	53°33 N	114°06 W	766	1961–70
Goose, Nfld.	53°18 N	60°22 W	36	1961–70
Maniwaki, Que.	46°22 N	75°59 W	170	1961–70
Moosonee, Ont.	51°16 N	80°39 W	10	1961–70
Nitchequon, Que.	53°12 N	70°54 W	539	1961–70
Port Hardy, B.C.	50°41 N	127°22 W	17	1961–70
Prince George, B.C.	53°53 N	122°41 W	676	1961–70
Sable Island, N.S.	43°56 N	60°01 W	4	1961–70
Sept-Iles, Que.	50°13 N	66°16 W	53	1961–70
The Pas, Man.	53°58 N	101°06 W	273	1961–70
U.S.				
Annette, AK	55°02 N	131°34 W	37	1946–55
Bismarck, ND	46°46 N	100°45 W	505	1946–55
Buffalo, NY	42°56 N	78°44 W	182	1946–55
Caribou, ME	46°52 N	68°01 W	191	1946–55
Glasgow, MT	48°13 N	106°37 W	648	1946–55
Great Falls, MT	47°29 N	111°22 W	1123	1946–55
International Falls, MN	48°34 N	93°23 W	360	1946–55
Northway, AK	63°00 N	141°55 W	524	1946–55
Sault Ste. Marie, MI	46°28 N	122°18 W	221	1946–55
Tatoosh Island, WA	48°23 N	124°44 W	31	1946–55

latitude sites in the northern U.S. and southern Canada during a noticeable part of the winter season.

For the present study, a reexamination of Reitan's analysis was therefore conducted, using a dataset of long-term average upper air soundings combining 11 sites in Canada and 10 bordering U.S. sites (Fig. 2, Table 1). The Canadian data [Titus (1973)] cover the period 1961–70 for soundings at 0000 and 1200 GMT, whereas the U.S. data are averages from the period 1946–55 for soundings at 0300 GMT [Ratner (1957)]. Total precipitable water was obtained from the radiosonde data at different levels using essentially the same reduction technique as presented in Hay (1970), and a new simple equation for the saturation water vapor pressure over water [Gueymard (1993a)]. The experimental water vapor scale height was determined from eqn (1), using measured surface values of T and R_H to solve eqn (2). A statistical analysis showed that the average H_v was about 2.2 km for $T > 270$ K, but increased sharply at low temperatures (Fig. 3). As no discernible effect of station's elevation, atmospheric pressure or vapor pressure on H_v was observed on this dataset, H_v could be expressed solely as a function of T:

$$H_v = 0.4976 + 1.5265\theta + \exp(13.6897\theta - 14.9188\theta^3) \quad (4)$$

where $\theta = T/T_0$ and $T_0 = 273.15$ K.

2.3 *Results*

Using the proposed model [eqns (1), (2), and (4)], w was computed for some cities among the list of 333 Canadian stations [Anon. (1984)] for which monthly averages of T and R_H are available for the period 1951–80. For most of these sites (269 total), the climatic averages of pressure, temperature, and humidity are tabulated for 0100, 0700, 1300, and 1900 Local Standard Time (only 1300 LST data were used here because the daily variation of w is small); the remaining sites (64 total) report synoptic data at 1200 and 1800 GMT. The derived monthly precipitable water values are displayed in Table 2. As could be expected, northern stations have low precipitable water totals during winter time (e.g., The Pas, Manitoba), whereas the summer maximum at the southernmost stations of Canada almost never exceeds 3 cm (e.g., Kingston, Ontario). As could be expected, different seasonal patterns are apparent between locations in a maritime climate (e.g., Vancouver, British Columbia) and those in a continental climate (e.g., Winnipeg, Manitoba).

A similar methodology was applied to derive w at a number of northern U.S. sites. Climatic normals of temperature and humidity for the period 1941–70 were used [Anon. (1980)]. An important difference with the Canadian normals is that the U.S. normals provide *daily averages* of temperature (maximum, minimum, and mean), and average relative humidity *at specific times*, corresponding to the standardized synoptic reports defined by the World Meteorological Organization (0000, 0600, 1200, and 1800 GMT). In order to

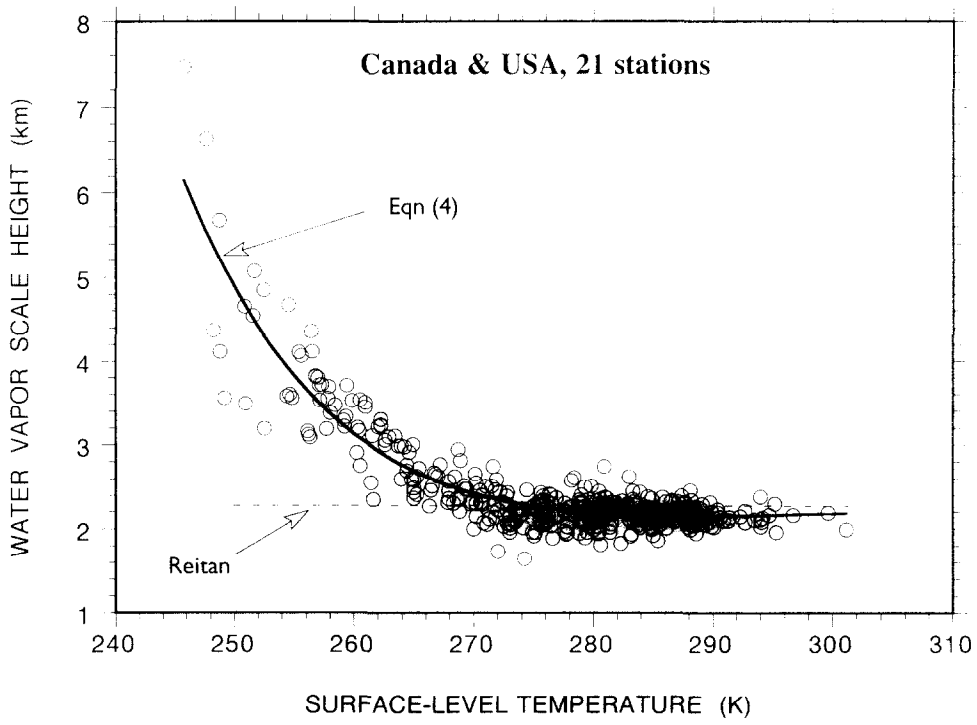

Fig. 3. Observed monthly-average water vapor scale height, H_v, as a function of surface-level temperature at 21 upper air stations in Canada and U.S.A.

Table 2. Monthly average precipitable water (in cm) calculated for 24 Canadian cities

Location	Month											
	1	2	3	4	5	6	7	8	9	10	11	12
Calgary, Alta.	0.45	0.57	0.66	0.85	1.11	1.50	1.77	1.74	1.33	0.94	0.67	0.54
Charlottetown, P.E.I.	0.64	0.63	0.80	1.02	1.45	2.15	2.71	2.65	2.05	1.49	1.12	0.78
Edmonton, Alta.	0.40	0.54	0.53	0.71	1.08	1.56	1.91	1.87	1.39	0.97	0.64	0.49
Goose, Nfld.	0.37	0.35	0.49	0.64	1.02	1.48	2.12	1.96	1.45	1.03	0.79	0.51
Halifax, N.S.	0.78	0.73	0.84	1.11	1.51	2.13	2.62	2.64	2.17	1.60	1.26	0.88
Kelowna, B.C.	0.74	0.92	0.93	1.00	1.36	1.76	2.00	1.97	1.74	1.33	1.06	0.86
Kingston, Ont.	0.59	0.60	0.83	1.12	1.75	2.45	3.04	2.97	2.28	1.57	1.10	0.71
London, Ont.	0.68	0.69	0.89	1.24	1.76	2.51	2.82	2.80	2.26	1.62	1.17	0.82
Moncton, N.B.	0.61	0.60	0.78	1.00	1.45	2.14	2.64	2.53	1.98	1.42	1.08	0.71
Montreal, Que.	0.51	0.53	0.72	1.08	1.60	2.41	2.77	2.65	2.08	1.42	1.00	0.61
Ottawa, Ont.	0.47	0.50	0.68	1.00	1.51	2.28	2.61	2.56	2.01	1.39	0.97	0.59
Port Hardy, B.C.	1.08	1.19	1.06	1.18	1.42	1.85	2.18	2.29	2.06	1.70	1.32	1.14
Quebec, Que.	0.48	0.50	0.67	0.94	1.40	2.17	2.59	2.49	1.88	1.28	0.90	0.56
Regina, Sask.	0.40	0.49	0.67	0.97	1.33	1.92	2.24	2.08	1.54	1.10	0.71	0.50
St. John, N.B.	0.60	0.60	0.77	1.02	1.45	2.11	2.56	2.50	1.95	1.44	1.07	0.72
St. Johns, Nfld.	0.77	0.75	0.85	1.02	1.31	1.79	2.36	2.34	1.86	1.43	1.17	0.88
Saskatoon, Sask.	0.36	0.46	0.62	0.92	1.25	1.76	2.12	1.99	1.47	1.05	0.67	0.47
Sherbrooke, Que.	0.50	0.48	0.67	0.92	1.44	2.27	2.63	2.56	1.93	1.31	0.95	0.60
Sydney, N.S.	0.75	0.69	0.84	1.05	1.45	2.11	2.70	2.67	2.12	1.58	1.22	0.88
The Pas, Man.	0.30	0.35	0.43	0.70	1.03	1.69	2.12	2.03	1.48	1.05	0.61	0.43
Thunder Bay, Ont.	0.40	0.44	0.63	0.90	1.28	1.97	2.44	2.41	1.81	1.26	0.79	0.49
Toronto, Ont.	0.65	0.68	0.86	1.16	1.65	2.38	2.71	2.70	2.19	1.56	1.13	0.79
Vancouver, B.C.	1.14	1.29	1.31	1.48	1.76	2.11	2.41	2.51	2.23	1.84	1.42	1.28
Winnipeg, Man.	0.38	0.45	0.64	0.97	1.36	2.05	2.52	2.32	1.65	1.20	0.74	0.47

obtain consistent datasets, the average daily mean temperature was corrected to obtain the average temperature at the same specific time for which humidity was used (humidity data closest to 1200 LST were chosen). The temperature correction, ΔT, added to the average daily mean temperature, T_a, is such that:

$$\Delta T = 2(T_M - T_a)\Omega \qquad (6)$$

where T_M is the average daily maximum temperature and Ω is a pseudo-sine function of time empirically obtained by Erbs *et al.* (1983). The derived monthly average precipitable water values are given in Table 3 for some northern U.S. cities.

For validation purpose, it is interesting to compare the estimates of w (using the proposed model) and observed data. This analysis has been performed for

Table 3. Monthly average precipitable water (in cm) calculated for 20 U.S. cities

Location	Month											
	1	2	3	4	5	6	7	8	9	10	11	12
Albany, NY	0.65	0.64	0.82	1.19	1.95	2.88	3.21	2.96	2.44	1.64	1.18	0.79
Anchorage, AK	0.56	0.65	0.66	0.89	1.21	1.79	2.13	2.11	1.60	1.02	0.73	0.60
Bismarck, ND	0.47	0.55	0.70	1.10	1.58	2.25	2.59	2.29	1.76	1.22	0.81	0.58
Boise, ID	0.83	0.96	0.97	1.11	1.42	1.71	1.90	1.75	1.52	1.29	1.09	0.92
Boston, MA	0.71	0.75	0.96	1.32	2.02	2.86	3.12	2.92	2.53	1.72	1.30	0.86
Chicago, IL	0.67	0.70	0.94	1.41	1.91	2.74	3.16	3.06	2.43	1.68	1.14	0.84
Fairbanks, AK	0.31	0.37	0.45	0.68	0.99	1.63	2.15	1.83	1.16	0.78	0.45	0.31
Glasgow, MT	0.45	0.56	0.68	1.01	1.29	1.74	2.16	1.88	1.48	1.08	0.80	0.58
Green Bay, WI	0.57	0.60	0.79	1.24	1.72	2.48	2.86	2.81	2.15	1.56	1.00	0.68
Madison, WI	0.57	0.63	0.81	1.25	1.81	2.54	2.93	2.90	2.26	1.54	1.00	0.71
Minneapolis, MN	0.50	0.55	0.77	1.21	1.79	2.49	2.94	2.84	2.19	1.56	0.91	0.63
Missoula, MT	0.71	0.86	0.91	1.09	1.36	1.77	1.92	1.82	1.74	1.38	1.03	0.81
New York, NY	0.81	0.83	1.03	1.44	2.13	2.97	3.45	3.38	2.74	1.90	1.34	0.91
Portland, ME	0.65	0.67	0.85	1.18	1.78	2.53	3.02	2.87	2.31	1.61	1.15	0.75
Saint Cloud, MN	0.48	0.52	0.72	1.09	1.61	2.37	2.80	2.80	2.00	1.42	0.85	0.59
Seattle, WA	1.09	1.22	1.29	1.45	1.69	2.27	2.35	2.15	1.80	1.40	1.22	0.75
Spokane, WA	0.75	0.90	0.93	1.04	1.25	1.47	1.59	1.61	1.44	1.27	1.05	0.87
Toledo, OH	0.75	0.78	1.01	1.47	2.00	2.88	3.20	3.23	2.60	1.72	1.21	0.89
Washington, DC	0.85	0.89	1.13	1.66	2.36	3.24	3.57	3.46	2.88	1.90	1.30	0.95
Youngstown, OH	0.82	0.83	1.05	1.47	1.98	2.79	3.06	2.93	2.50	1.74	1.25	0.91

nine pairs of bordering Canadian and U.S. sites. Monthly average measured precipitable water data in the U.S. were taken from tabulated results in various sources [Lott (1976), NREL (1992), Reitan (1960)] or processed from average temperature and humidity profiles [Ratner (1957)]. Some data were also derived from the proposed model, using U.S. climatic normals [Anon. (1980)]. The agreement has been found generally very good, considering the various sources of inaccuracy of such a procedure. One particularly interesting case has been chosen as an illustration, and appears in Table 4. The site is Sault Ste. Marie, a city that has its banks on either side of the Canada/U.S. border. The distance between the radiosonde site (on the U.S. side) is therefore ideally close from the Canadian side, where w has been estimated from climatological data. The derived data using the Canadian climatological normals (1951–80) appear in reasonably close agreement with the monthly average observed data (Table 4).

2.4 *Short-term fluctuations and their significance*

Although it is known that there is some year-to-year variability of the monthly average w, it is generally assumed that this variability is of limited importance when modeling solar radiation, because of the saturation effect in the transmittance of water vapor. However, it could be argued that the accuracy of w may have more impact on the accuracy of the modeled solar radiation in winter at northern continental sites where precipitable water is extremely low, allowing little saturation effect. For example, Fig. 4 illustrates the high variability of precipitable water that can be expected in the case of a continental climate. Nineteen years of monthly average data (1961–79) at Nitchequon, Quebec, for the normally coldest (January) and warmest (July) months of the year were used. On top of the quite high year-to-year variability apparent in Fig. 4, there is also a high day-to-day variability. Figure 5 shows an example of the daily excursions of precipitable water at 0000 GMT for the relatively "dry" month of January 1961 at Nitchequon (mean w = 0.16 cm). Figure 5 also shows the corresponding variability of the water vapor absorptance, as calculated by a clear-sky two-band radiation model [Gueymard (1989)], using a solar elevation of 11.5° (close to the maximum possible in January at this latitude, and corresponding to a water vapor optical mass of 5.0). The daily course of w appears extremely erratic, with extreme values 20% and 275% of its observed monthly mean (with a coefficient of variation of 63.2%). Despite the efficient saturation effect, the corresponding extremes of the water vapor absorptance are still significantly different (82% and 116%, respectively, with a coefficient of variation of 7.8%) from the calculated monthly mean. These findings suggest that precipitable water variability may have slight—but discernible—effects on solar radiation in cold climates.

3. ATMOSPHERIC TURBIDITY

Atmospheric turbidity describes the ability of natural or anthropogenic aerosols to scatter and absorb solar radiation. Turbidity is related to the aerosol optical thickness which varies on a seasonal basis, and even from one day to the next, depending on the type (or provenance) of aerosols, size distribution of the particles, and the possible presence of volcanic dust/droplet clouds in the stratosphere.

3.1 *Existing data*

For the U.S., tabulated monthly average turbidity data are available from only a few sources. The seasonal turbidity variations at 26 stations for the period 1960–66 were provided by Flowers *et al.* (1969), but only in graphical form. The WMO turbidity network data [WMO (1971)] for 27 stations and the period 1971–73 were processed to derive the SOLMET data [Quinlan (1979)], and those monthly turbidity data were later reproduced in a classic textbook [Iqbal (1983)]. Other data may be given in some environmental study at a specific site [e.g., Peterson and Flowers (1977)], but most turbidity data users may have difficulty to locate them.

Previously, very little information has been available on the monthly turbidity regime in Canada. The available datasets have generally been obtained from indirect solar radiation measurements at a few sites. For example, Latimer (1974) and Yamashita (1974) used radiometric measurements to derive turbidity data for Toronto city and its suburbs. Latimer's results were somewhat biased toward low turbidities because most

Table 4. Comparison of calculated precipitable water at Sault Ste. Marie, Ont. [using eqns (1), (2), and (4), and climatic normals 1951–80] to radiosonde data at Sault Ste. Marie, MI

	Month											
Location	1	2	3	4	5	6	7	8	9	10	11	12
Sault Ste. Marie, Ont.	0.53	0.53	0.70	0.99	1.41	2.12	2.49	2.49	1.98	1.40	0.97	0.65
Sault Ste. Marie, MI (1)	0.56	0.54	0.64	0.98	1.39	2.19	2.50	2.46	1.93	1.52	0.92	0.63
Sault Ste. Marie, MI (2)	0.56	0.54	0.65	0.99	1.41	2.15	2.52	2.45	1.94	1.48	0.90	0.63
Sault Ste. Marie, MI (3)	0.59	0.56	0.68	1.00	1.44	2.11	2.34	2.35	1.98	1.48	0.98	0.70
Sault Ste. Marie, MI (4)	0.50	0.51	0.68	0.98	1.46	2.02	2.37	2.34	1.95	1.36	0.93	0.61

(1) Averages 1946–56 [Reitan (1960)]; (2) averages 1946–55, processed from Ratner (1957); (3) averages 1946–72 [Lott (1976)]; (4) averages 1961–90 [NREL (1992)].

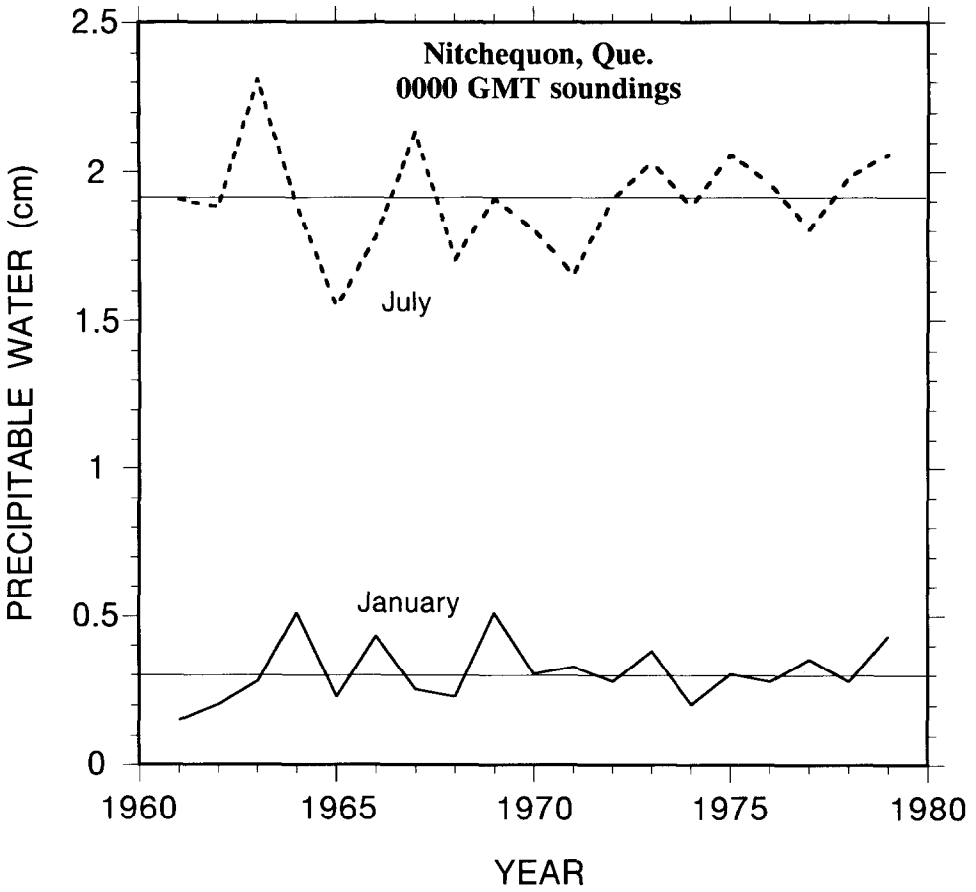

Fig. 4. Time series of monthly-average precipitable water for the normally coldest and warmest months at Nitchequon, Quebec, Canada, 1961–79. Thin horizontal lines: long-term averages.

of the measurements were done during very clear days, following the passage of a cold front. The original measurements analyzed by Latimer (1974) and Yamashita (1974) were done between 1956 and 1971, and therefore, may not be representative of the current aerosol climatology of Toronto, a semi-industrial city that has grown significantly from that period.

Sadler (1978) used a filtered pyrheliometer to derive monthly average values of different turbidity coefficients (Angström's β, Linke's T_L, and Schüepp's B) for the period 1973–76 in Edmonton. Sadler also compared these radiometric (indirect) determinations of turbidity to measurements of the aerosol optical thickness at 0.5 μm, τ_{a5}, using a Volz sunphotometer. The disagreement between B and τ_{a5} was noticeable, suggesting potential errors in the measurement or reduction technique of one (or both) of the data sets.

Polavarapu (1978) used a method similar to Yamashita (1974) to derive T_L from measured hourly data of global and diffuse radiation at Goose, Montreal, Resolute, and Toronto during the period 1966–71. As only periods of high solar transmittance and only the 25 lowest observed values of T_L in a given month were retained, the monthly average turbidity values are almost certainly underestimated.

Freund (1983) used Davies and Hay's clear-sky radiation model [Davies and Hay (1980)] to derive the Unsworth–Monteith's broadband aerosol optical depth, τ_a, at five arctic stations for the period 1978–80. Diffuse radiation was not available at four of the stations, so τ_a had to be derived from global radiation data only. As global radiation is only weakly dependent on turbidity (comparatively to beam radiation), this process may not necessarily provide accurate hourly turbidity estimates. However, the monthly average turbities derived by Freund appeared consistent with other published data for Alaska [Freund (1983)].

Uboegbulam and Davies (1983) also used the Davies and Hay (1980) radiation model to derive the monthly averages of τ_a at Goose, Montreal, and Toronto-Woodbridge. Measured data on hourly global and diffuse radiation for the period 1968–78 were used.

Hay and Darby (1984) used hourly pyrheliometric beam radiation data measured at Vancouver during the period 1977–83. Turbidity coefficient τ_a was derived from the Davies–Hay model, with a methodology similar to previously cited studies. A very significant increase of turbidity was shown to have taken place about 6 months after the El Chichon volcano erupted in April 1982.

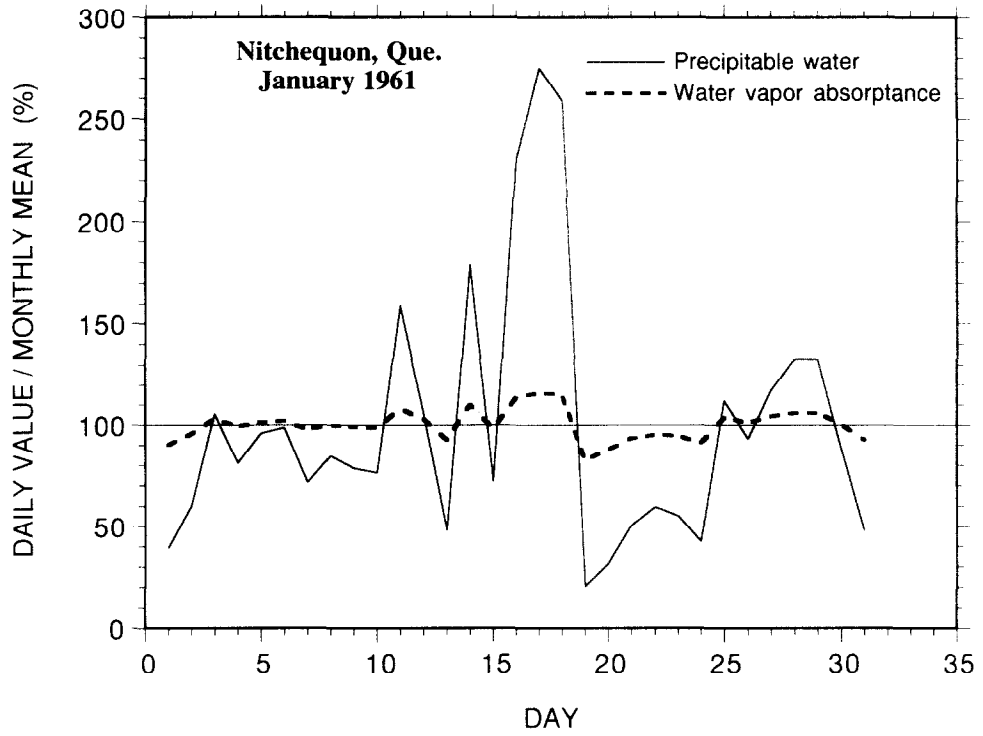

Fig. 5. Daily excursions of precipitable water and water vapor absorptance around their respective mean for January, 1961 at Nitchequon, Quebec, Canada.

Finally, Garrison and Sahami (1993) used hourly global and diffuse radiation data, as well as related meteorological data, at Edmonton, Montreal, Port Hardy, Toronto, and Winnipeg, for periods of 7–20 yr ending in 1984. They derived the hourly value of β using the method of Louche *et al.* (1987). It is hoped that corresponding data of monthly average turbidity will be derived from this dataset in the near future [personal communication with J. D. Garrison (1993)].

Most of the studies described above suffer from evident methodological limitations, the most important of which are the use of an indirect method to obtain turbidity from broadband radiation observations, and the *a posteriori* selection of clear days or clear hours, that may not be representative of the general aerosol regime. It is not known if the effect of the former factor is to introduce a systematic bias (as would suggest the comparison made by Sadler [1978]) or only random noise. The effect of the latter factor would be to underestimate the average turbidity because very clear periods tend to be selected.

3.2 *Analysis of the WMO dataset*

A network of turbidity measurement stations was established by the World Meteorological Organization (WMO) and its members in 1971. Although this network is relatively scarce around the world, a large proportion of its stations were located in Canada and the U.S. However, no recent data are available as these two countries stopped reporting measurements in 1986 and 1985, respectively. The stations used in this study (Table 5 and Fig. 2) comprise all of the Canadian network, and some U.S. bordering stations.

All WMO data were obtained through measurement of the aerosol optical thickness at 0.5 μm and 0.38 μm (the latter wavelength not reported at all stations or in the first years, however). The spectral aerosol optical thickness, $\tau_{a\lambda}$, is classically obtained from the irradiance, E_λ, at wavelength λ, which is proportional to the meter deflection indicated by the sunphotometer (the proportionality constant being determined during calibration by the "Langley method"):

$$\tau_{a\lambda} = -(1/m)\ln(E_\lambda/E_{0\lambda}) - \tau_{R\lambda} - \tau_{O\lambda} \qquad (6)$$

where m is the relative optical air mass, $E_{0\lambda}$ is the extraterrestrial irradiance at the actual sun–earth distance, $\tau_{R\lambda}$ is the optical thickness for Rayleigh scattering, and $\tau_{O\lambda}$ is the optical thickness for ozone absorption.

The aerosol optical thickness at wavelength λ is also classically expressed in terms of the optical thickness at 1 μm, β, using Angström's equation:

$$\tau_{a\lambda} = \beta\lambda^{-\alpha} \qquad (7)$$

where β is known as the Angström turbidity coefficient, α is Angström's wavelength exponent, and λ is in micrometers. This equation may be rewritten:

$$\beta = k_1\tau_{a5} \qquad (8)$$

Table 5. Turbidity stations of the WMO network used in the present study

Station	Latitude	Longitude	Alt. (m)	Period
Canada				
Armstrong, Ont.	50°17 N	88°54 W	322	1974–77
Edson, Alta.	53°35 N	116°27 W	924	1974–86
Fort Simpson, NWT	61°45 N	121°14 W	170	1974–78
Kelowna, B.C.	49°58 N	119°23 W	417	1977–83
Maniwaki, Que.	46°23 N	75°58 W	170	1975–82
Mount Forest, Ont.	43°59 N	80°45 W	414	1973–79
Pickle Lake, Ont.	51°28 N	90°12 W	373	1977–83
Puntzi Mountain, B.C.	52°07 N	124°05 W	911	1975–77
Sable Island, N.S.	43°56 N	60°01 W	4	1975–81
Wynyard, Sask.	51°46 N	104°12 W	561	1974–84
U.S.				
Bismarck, ND	46°46 N	100°45 W	506	1974–85
Caribou, ME	46°52 N	68°01 W	191	1971–85
Green Bay, WI	44°29 N	88°08 W	210	1971–80
Missoula, MT	46°55 N	114°05 W	980	1971–82
Saint Cloud, MN	45°33 N	94°04 W	314	1971–82
Toledo, OH	41°39 N	83°32 W	181	1971–78
Youngstown, OH	41°16 N	80°40 W	365	1971–84

where $k_1 = 0.5^{\alpha}$. When measurements at only one wavelength (i.e., 0.5 μm) are available, α is assumed to be constant at 1.3, so that k_1 reduces to 0.406. When measurements at two wavelengths are available (in the present case, $\lambda_1 = 0.5$ μ and $\lambda_2 = 0.38$ μm), α is derived assuming it is constant throughout the spectrum:

$$\alpha = \ln(\tau_{a\lambda 2}/\tau_{a\lambda 1})/\ln(\lambda_1/\lambda_2) \qquad (9)$$

This reduction technique has always been used in the WMO publications [WMO (1971)], with the exception that, prior to 1979, $\tau_{a\lambda}$ was defined on the decimal logarithm scale in eqn (6).

Schüepp's turbidity coefficient, B, can be simply derived from τ_{a5} through:

$$B = k_2\tau_{a5} \qquad (10)$$

with $k_2 = 1/\ln 10 = 0.434$. The correspondence between B and β is obtained by combining (8) and (10):

$$B = (k_2/k_1)\beta \qquad (11)$$

No exact relationship exists between τ_a or T_L and τ_{a5}, β, or B (τ_a and T_L are in fact not pure turbidity coefficients as for a given aerosol optical thickness, they vary with the air mass, m). Approximate empirical relationships have been proposed however; see, for example, Dogniaux (1975), Grenier *et al.* (1994), Uboegbulam and Davies (1983), and Valko (1967), thus allowing for the cross-estimation of the various turbidity coefficients. This possibility is important because all of them are used in the literature, and radiation models use one or the other.

Although the WMO network uses turbidity measurements of a "direct" nature (i.e., the aerosol optical thickness is determined using spectral data where no strong atmospheric absorption exists), they are subject to possibly important errors. A recent study [Gueymard (1993b)] showed that the WMO data set could include erroneous data for periods of up to a few months, but some simple *a posteriori* screening improves their consistency. The typical errors may result from:

- Cloud interference (e.g., from subvisual cirrus).
- Sunphotometer misalignment.
- Improper calibration (e.g., due to temporal variations in turbidity [Shaw (1976a)].
- Drift or loss of calibration due to various factors (filter degradation in particular).
- Parasitic diffuse radiation in the field of view of the instrument [Shah (1978)].
- Presence of stratospheric and tropospheric NO_2, that absorbs significantly between about 0.3 and 0.6 μm (this parasitic effect can be of significant importance in urban environments, particularly at the low turbidities frequently encountered in winter in cold climates [Schroeder and Davies (1987), Shaw (1976b)].

Finally it has been shown [Cachorro *et al.* (1987)] that the derivation of α through eqn (9) may be biased because it is not necessarily constant throughout the spectrum. In many instances, α shows some curvature as a function of λ, with low or even negative values below 0.4 μm. Therefore, the extrapolation from 0.5 to 1.0 μm, necessary to obtain β from τ_{a5}, may be inaccurate when α is determined as an average between 0.38 and 0.5 μm as is the case in the WMO data.

3.3 *Results*

The whole dataset has been first screened for anomalous individual data. No really obvious error was observed in Canada, although incidental occurrences of very high (>3.0) values of α, or, more frequently, of very low values (<0.0) are noticeable. These values can result from real aerosol conditions (e.g., large aerosol particles, high volcanic loading, severe pollution events, etc.), instrumental errors, or from a

too-simplistic reduction technique, as explained above. Among the U.S. stations analyzed, limited problems were identified at Missoula and Bismarck. Excessively high optical thicknesses were reported at Missoula (where a single-wavelength sunphotometer was in use) during the summer of 1976 and summer/autumn of 1981, and they were eliminated. Anomalous data were also apparent at Bismarck in 1983, but corrected values were published later in the 1987/88 edition of the WMO reports [WMO (1971)].

From the preceding section, it is clear that two different determinations of β can be proposed, depending if eqn (8) is used with $\alpha = 1.3$ or with the apparent value of α, as obtained from a dual-wavelength sunphotometer. Although in theory it seems better to retain the observed value of α to derive β, such a derivation may be erroneous if α itself is in error. Furthermore, the data from some sites (e.g., Missoula) may only be analyzed if $\alpha = 1.3$ is assumed. Many international turbidity estimates as well as radiation models also assume that $\alpha = 1.3$. Therefore, even if β obtained with $\alpha = 1.3$ is not the "true" value, it is a very convenient way to present data and compare datasets between them. This "reduced" value (using $\alpha = 1.3$) of β will be noted β^* in what follows.

The observed variation of α with time at the different stations considered in this study (as outlined in Fig. 6 for two stations) show that its overall average is generally close to 1.3, although the variance around this value is quite high. When turbidity is low (which is particularly the case in winter at northern sites), the influence of stratospheric aerosols may become noticeable. After a major volcanic eruption, a considerable amount of dust and aerosol-forming gases are released into the stratosphere. The resulting aerosols generally consist of large particles, so that there is only weak wavelength dependency of their optical thickness (i.e., their α is close to 0.0 and may even be slightly negative).

From Fig. 6, it appears that records at Edson and Caribou show a very significant decrease of α, which started around 1982. This can be attributed in great part to the influence of the El Chichon eruption. Although regular volcanic activity occurred throughout the measurement period (Fig. 6), the El Chichon eruption was one of the most important of the century, climate-wise. Significant effects on solar radiation were detected all around the world, and particularly in Vancouver [Hay and Darby (1984)] and the Pacific Northwest [Vignola and McDaniels (1985)]. The reported perturbation lasted a few years, so that it may explain the drop of α at Edson and the concomitant increase of τ_{a5} and β^* at all stations in 1982–85 (Figs. 6–8). Figures 7 and 8 show that the increase of turbidity in 1982–85 affected the winter values (that approximately doubled in 1982 compared to the previous years) more than the summer values. This recursive pattern with time decay is consistent with findings in specific studies [Vignola and McDaniels (1985), Yue *et al.* (1991)].

Figure 7 also shows a spike of turbidity at U.S. stations following the eruption of Mount St. Helens in May 1980. This effect was short lived and not even very apparent in Canada, because this eruption was of far less magnitude than El Chichon's. Conversely, it is known that turbidity increased very significantly after

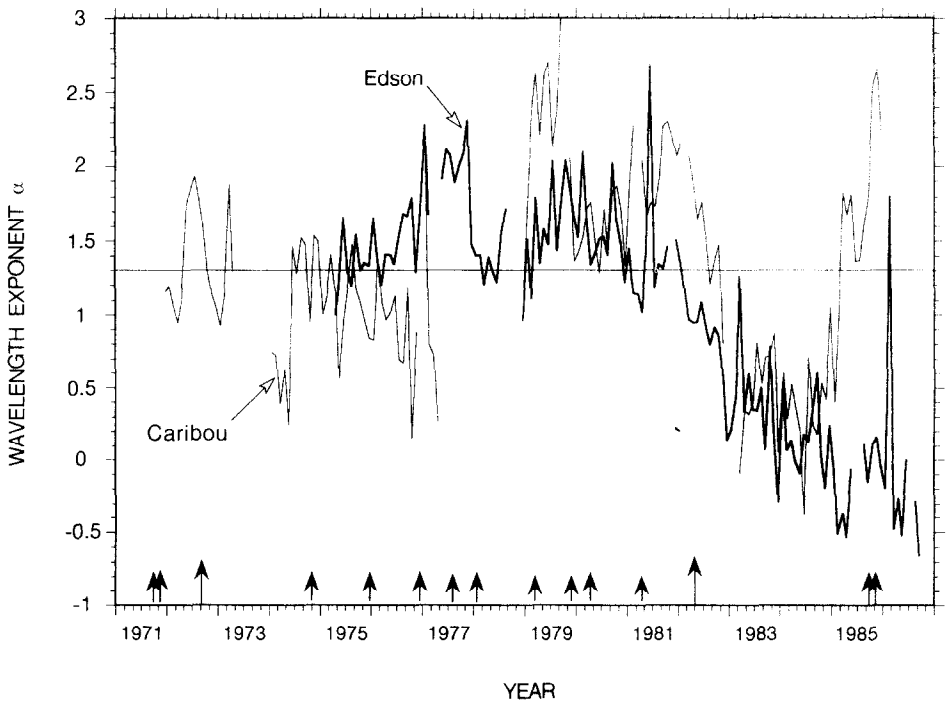

Fig. 6. Time series of the monthly-average wavelength exponent of turbidity at Edson and Caribou. Arrows indicate volcanic eruptions.

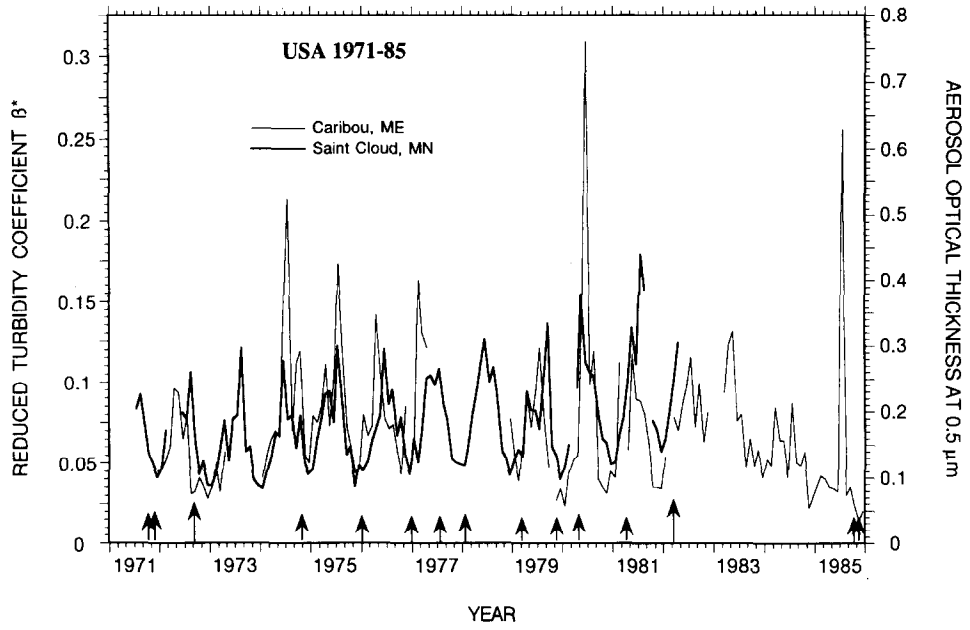

Fig. 7. Time series of reduced turbidity coefficient β^* and optical thickness τ_{a5} at two U.S. stations. Arrows indicate volcanic eruptions.

the eruption of Mt. Pinatubo in June 1991. This eruption was of larger magnitude than El Chichon and led to a 50% increase in stratospheric extinction compared to El Chichon's [Michalsky *et al.* (1993)]. Although this effect could not be studied with the North American WMO network data used here, it is important to consider it in order to adjust the turbidity average data for present conditions.

The monthly average turbidity derived from the WMO data is presented in Table 6 for each station. Due to the different recording periods (Table 5), these averages are not necessarily comparable: those stations with data including the post-El Chichon period tend to exhibit higher turbidities and lower wavelength exponents than the long-term "normal" (that remain to be defined). The results obtained for Green Bay, St. Cloud, and Youngstown are almost identical to those displayed (in terms of Schüepp's B) in an older study [Flowers *et al.* (1969)]. In Canada, Table 6 also indicates extremely low turbidities with minimal seasonal effects at Puntzi Mountain and Fort Simpson, contrasting with the high summer peaks and seasonal variations at Pickle Lake and Wynyard. The total number of data days (ND) and data months (NM) are indicated

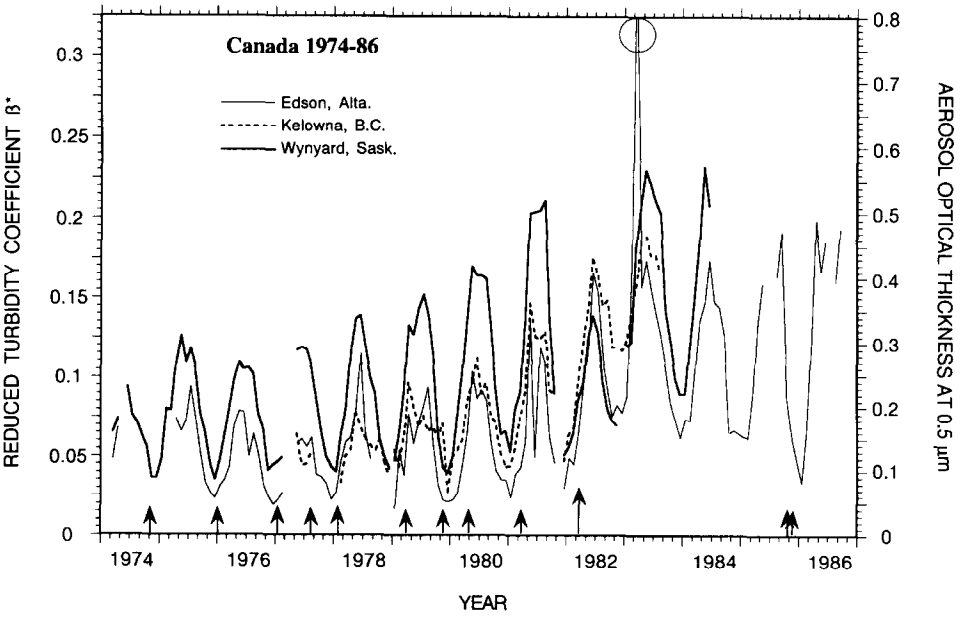

Fig. 8. Time series of reduced turbidity coefficient β^* and optical thickness τ_{a5} at three Canadian stations. The circled peak corresponds to a single measurement during March, 1983. Arrows indicate volcanic eruptions.

Table 6. Monthly average turbidity parameters β, β^*, τ_{a5}, and α, number of data days (ND), and number of data months (NM) for the WMO network

Location		Month 1	2	3	4	5	6	7	8	9	10	11	12
Canada													
Armstrong	$10^3\beta$ ($10^3\beta^*$)	52 (49)	63 (61)	86 (79)	105 (95)	126 (114)	124 (123)	120 (117)	104 (109)	60 (78)	53 (65)	49 (57)	49 (46)
	$10^3\tau_{a5}$ (α)	120 (1.25)	150 (1.29)	193 (1.15)	234 (1.20)	280 (1.16)	302 (1.31)	288 (1.26)	268 (1.39)	191 (1.71)	161 (1.60)	140 (1.53)	113 (1.20)
	ND (NM)	19 (3)	18 (2)	28 (3)	34 (3)	34 (3)	19 (3)	37 (3)	35 (3)	21 (3)	7 (2)	16 (3)	25 (3)
Edson	$10^3\beta$ ($10^3\beta^*$)	67 (41)	91 (58)	148 (92)	190 (100)	196 (113)	162 (111)	129 (100)	166 (104)	191 (94)	75 (53)	81 (47)	72 (39)
	$10^3\tau_{a5}$ (α)	101 (1.06)	144 (1.07)	227 (1.04)	246 (0.91)	277 (0.93)	272 (1.24)	247 (1.26)	255 (1.01)	231 (1.01)	132 (1.21)	116 (1.00)	116 (0.90)
	ND (NM)	82 (11)	54 (11)	60 (11)	97 (12)	123 (12)	129 (11)	130 (10)	142 (12)	94 (11)	90 (10)	75 (9)	59 (11)
Fort Simpson	$10^3\beta$ ($10^3\beta^*$)	53 (48)	56 (44)	69 (55)	71 (62)	59 (59)	65 (59)	75 (59)	66 (64)	54 (47)	36 (34)	33 (23)	—
	$10^3\tau_{a5}$ (α)	119 (1.44)	109 (0.77)	136 (1.00)	152 (1.10)	146 (1.36)	146 (1.18)	146 (0.95)	157 (1.26)	115 (1.08)	84 (1.21)	58 (0.79)	—
	ND (NM)	15 (3)	32 (4)	32 (4)	37 (4)	31 (4)	24 (4)	29 (4)	16 (3)	12 (3)	7 (3)	7 (2)	0 (0)
Kelowna	$10^3\beta$ ($10^3\beta^*$)	96 (67)	93 (65)	125 (84)	168 (106)	170 (114)	178 (111)	171 (106)	156 (102)	100 (88)	89 (80)	99 (72)	86 (54)
	$10^3\tau_{a5}$ (α)	165 (1.00)	161 (1.06)	207 (1.06)	261 (0.92)	281 (1.09)	272 (1.15)	260 (1.23)	251 (1.20)	216 (1.29)	198 (1.37)	177 (1.20)	132 (1.01)
	ND (NM)	9 (5)	25 (6)	47 (6)	47 (6)	70 (7)	84 (7)	95 (7)	109 (7)	48 (5)	53 (5)	20 (4)	17 (5)
Maniwaki	$10^3\beta$ ($10^3\beta^*$)	71 (53)	82 (62)	86 (74)	101 (90)	118 (107)	102 (97)	112 (103)	89 (82)	63 (62)	56 (54)	57 (51)	63 (53)
	$10^3\tau_{a5}$ (α)	131 (0.93)	153 (0.94)	182 (1.12)	222 (1.26)	264 (1.22)	239 (1.26)	254 (1.23)	201 (1.20)	153 (1.40)	132 (1.27)	124 (1.12)	130 (1.05)
	ND (NM)	75 (6)	58 (6)	58 (5)	63 (5)	79 (7)	81 (7)	88 (6)	80 (6)	51 (5)	51 (6)	33 (5)	51 (6)
Mount Forest	$10^3\beta$ ($10^3\beta^*$)	40 (44)	47 (46)	80 (82)	96 (96)	129 (118)	128 (108)	111 (112)	103 (112)	52 (65)	56 (69)	34 (42)	30 (42)
	$10^3\tau_{a5}$ (α)	109 (1.51)	113 (1.54)	202 (1.63)	236 (1.52)	290 (1.24)	266 (1.17)	276 (1.43)	276 (1.49)	159 (1.81)	169 (1.63)	104 (1.76)	103 (1.85)
	ND (NM)	11 (3)	27 (3)	25 (3)	30 (4)	35 (4)	44 (4)	43 (5)	40 (5)	23 (4)	37 (4)	12 (4)	6 (3)
Pickle Lake	$10^3\beta$ ($10^3\beta^*$)	—	82 (88)	97 (111)	110 (138)	135 (167)	124 (162)	120 (153)	98 (133)	73 (103)	51 (71)	44 (57)	—
	$10^3\tau_{a5}$ (α)	—	218 (1.45)	272 (1.50)	340 (1.61)	412 (1.60)	398 (1.69)	378 (1.69)	327 (1.82)	254 (1.87)	175 (1.90)	139 (1.66)	—
	ND (NM)	0 (0)	15 (5)	67 (6)	72 (5)	76 (6)	73 (6)	79 (6)	68 (6)	57 (6)	40 (6)	12 (4)	0 (0)
Puntzi Mtn.	$10^3\beta$ ($10^3\beta^*$)	17 (18)	30 (27)	41 (37)	54 (49)	74 (68)	33 (43)	32 (47)	40 (51)	22 (32)	9 (21)	—	29 (23)
	$10^3\tau_{a5}$ (α)	45 (1.45)	67 (1.17)	92 (1.16)	120 (1.14)	168 (1.21)	105 (1.74)	116 (1.87)	125 (1.67)	79 (1.87)	51 (2.44)	—	58 (1.13)
	ND (NM)	11 (2)	10 (1)	13 (1)	15 (1)	16 (2)	11 (2)	14 (2)	18 (2)	27 (2)	5 (1)	0 (0)	6 (2)

	$10^3\beta$ ($10^3\beta^*$)	86 (73)	101 (82)	112 (87)	144 (114)	161 (115)	135 (99)	183 (127)	143 (93)	144 (96)	132 (90)	78 (63)	89 (64)
Sable Island	$10^3\tau_{a5}$ (α)	179 (1.06)	201 (1.00)	215 (0.97)	280 (0.96)	283 (0.82)	243 (0.92)	313 (0.82)	229 (0.78)	236 (0.79)	222 (0.88)	156 (1.02)	158 (0.93)
	ND (NM)	9 (3)	27 (4)	44 (6)	32 (6)	47 (5)	44 (6)	27 (7)	35 (6)	51 (5)	31 (5)	18 (5)	15 (5)
	$10^3\beta$ ($10^3\beta^*$)	95 (60)	132 (79)	165 (101)	209 (129)	260 (158)	251 (150)	214 (140)	195 (130)	148 (99)	107 (76)	83 (55)	72 (50)
Wynyard	$10^3\tau_{a5}$ (α)	147 (0.77)	194 (0.66)	248 (0.71)	319 (0.72)	388 (0.69)	368 (0.67)	344 (0.77)	319 (0.78)	244 (0.78)	186 (0.87)	136 (0.85)	122 (0.86)
	ND (NM)	107 (10)	110 (10)	144 (10)	157 (10)	166 (10)	184 (10)	209 (10)	176 (10)	155 (10)	141 (10)	93 (9)	106 (9)
U.S.													
	$10^3\beta$ ($10^3\beta^*$)	52 (35)	120 (63)	95 (58)	125 (77)	118 (85)	112 (83)	96 (81)	105 (78)	93 (64)	73 (47)	74 (42)	63 (40)
Bismarck	$10^3\tau_{a5}$ (α)	87 (1.00)	154 (0.79)	141 (0.67)	190 (0.68)	209 (0.78)	204 (0.94)	200 (1.21)	191 (0.90)	157 (0.85)	116 (0.80)	103 (0.54)	99 (0.92)
	ND (NM)	87 (9)	90 (10)	82 (9)	101 (10)	121 (10)	133 (10)	162 (10)	158 (10)	153 (10)	121 (10)	87 (10)	92 (9)
	$10^3\beta$ ($10^3\beta^*$)	56 (51)	77 (68)	92 (71)	107 (84)	107 (88)	108 (104)	123 (126)	72 (70)	60 (61)	63 (52)	50 (44)	47 (41)
Caribou	$10^3\tau_{a5}$ (α)	124 (1.25)	167 (1.24)	176 (1.26)	207 (1.21)	217 (1.21)	256 (1.30)	309 (1.38)	173 (1.34)	150 (1.52)	129 (1.30)	109 (1.39)	100 (1.25)
	ND (NM)	94 (12)	78 (11)	86 (12)	81 (13)	61 (11)	52 (11)	52 (11)	67 (11)	42 (11)	51 (10)	35 (11)	61 (11)
	$10^3\beta$ ($10^3\beta^*$)	87 (57)	95 (67)	128 (85)	156 (111)	171 (114)	155 (107)	152 (113)	131 (102)	102 (71)	80 (62)	81 (56)	63 (44)
Green Bay	$10^3\tau_{a5}$ (α)	140 (0.90)	164 (0.80)	209 (0.75)	273 (0.81)	281 (0.71)	264 (0.77)	277 (0.86)	250 (0.94)	176 (0.82)	152 (1.01)	139 (0.81)	109 (0.81)
	ND (NM)	101 (9)	84 (9)	71 (9)	84 (8)	90 (8)	88 (8)	117 (9)	88 (9)	115 (10)	89 (10)	77 (9)	64 (8)
	β (β^*)	— (40)	— (50)	— (53)	— (74)	— (61)	— (60)	— (58)	— (57)	— (61)	— (47)	— (69)	— (37)
Missoula	$10^3\tau_{a5}$ (α)	124 (—)	140 (—)	122 (—)	243 (—)	195 (—)	221 (—)	274 (—)	200 (—)	233 (—)	148 (—)	282 (—)	90 (—)
	ND (NM)	18 (7)	23 (8)	23 (7)	46 (8)	56 (9)	63 (9)	107 (10)	89 (10)	103 (11)	72 (10)	18 (8)	19 (8)
	$10^3\beta$ ($10^3\beta^*$)	51 (48)	62 (59)	74 (70)	88 (92)	91 (97)	105 (100)	98 (99)	106 (104)	87 (76)	62 (62)	56 (52)	49 (44)
Saint Cloud	$10^3\tau_{a5}$ (α)	182 (1.24)	223 (1.23)	255 (1.25)	359 (1.38)	380 (1.48)	343 (1.35)	346 (1.38)	361 (1.33)	260 (1.17)	212 (1.34)	181 (1.25)	150 (1.19)
	ND (NM)	142 (11)	112 (11)	86 (9)	102 (10)	91 (9)	103 (10)	138 (11)	127 (11)	131 (10)	113 (11)	96 (11)	81 (11)
	$10^3\beta$ ($10^3\beta^*$)	67 (61)	72 (66)	124 (84)	114 (93)	151 (116)	130 (139)	145 (176)	99 (146)	92 (105)	75 (89)	58 (61)	56 (57)
Toledo	$10^3\tau_{a5}$ (α)	150 (1.27)	163 (1.43)	208 (0.82)	228 (1.03)	284 (1.08)	343 (1.08)	434 (1.08)	358 (1.23)	259 (1.49)	220 (1.44)	151 (1.46)	140 (1.31)
	ND (NM)	46 (7)	54 (7)	54 (6)	69 (6)	68 (6)	44 (6)	97 (6)	60 (6)	71 (7)	65 (7)	50 (7)	36 (7)
	$10^3\beta$ ($10^3\beta^*$)	232 (103)	215 (113)	265 (142)	323 (173)	365 (190)	367 (213)	381 (238)	402 (235)	297 (168)	215 (123)	267 (119)	206 (97)
Youngstown	$10^3\tau_{a5}$ (α)	254 (0.53)	279 (0.65)	350 (0.72)	427 (0.70)	468 (0.75)	525 (0.75)	587 (0.78)	579 (0.72)	414 (0.67)	302 (0.74)	294 (0.50)	240 (0.55)
	ND (NM)	52 (13)	66 (12)	80 (12)	119 (13)	93 (12)	96 (12)	87 (11)	75 (11)	87 (13)	88 (11)	58 (12)	43 (11)

in Table 6 because their seasonal and station-to-station variations may explain a part of the difference in turbidity regimes. More clear days are observed during summertime, thus leading to more representativity of the summer data from a purely statistical standpoint. The higher the ND and NM the higher the confidence that can be placed in the results of Table 6.

4. CONCLUSION

Basic monthly average precipitable water and atmospheric turbidity data have been derived for a number of Canadian and U.S. sites. These data may be used in a variety of applications dealing with solar radiation, daylight availability, and pollution trends.

At neighboring stations along the Canada/U.S. border, precipitable water data generated on the Canadian side with the revised scale height model proposed here agree well with published U.S. monthly data. Similar data can be generated at all sites where climatological daily averages of temperature and humidity are available, for a total of about 640 stations for the U.S. and Canada combined.

Turbidity data are more difficult to obtain and have been very scarce in all countries. Estimates of turbidity are available for a few cities where solar radiation is measured. The WMO turbidity network has produced relatively long series of data at a few other sites, an analysis of which has been presented. The monthly average turbidity results presented may be used in a variety of applications, thanks to simple interrelationships (also reviewed) between the different turbidity coefficients.

Significant influence of the El Chichon eruption (1982) is apparent in the records, so that great care is necessary when long-term turbidity averages are estimated over periods with different volcanic activity.

A generalization and assessment of the proposed precipitable water model is underway using more input data, to check its validity in the various climates of the U.S. and Mexico, as well as its validity to estimate specific hourly values. Further studies will be necessary to improve the accuracy and to extend the spatial coverage (including urban and nonurban sites) of turbidity data.

Acknowledgments—The author wishes to thank Dr. Joseph Michalsky and Dr. Eric P. Shettle who provided helpful comments and documents regarding the volcanic effects on turbidity. Dr. Richard Leduc kindly provided some detailed precipitable water data for Canada. Dr. Ross McCluney was particularly instrumental in reviewing the manuscript.

REFERENCES

Anderson, G. P., Clough, S. A., Kneizys, F. X., Chetwynd, J. H., and Shettle, E. P., AFGL atmospheric constituent profiles (0–120 km), Tech. Rep. AFGL-TR-86-0110, Air Force Geophysics Lab, Hanscom AFB, MA (1986).

Anon., *U.S. Standard Atmosphere supplements, 1966*, ESSA/NASA/USAF, U.S. Government Printing Office, Washington, DC (1966).

Anon., *Climate of the States* (2nd ed.), Gale Research Co., Detroit, MI (1980).

Anon., *Canadian climate normals 1951–1980*, Vol. 8: *Atmospheric pressure, temperature, and humidity*, Atmospheric Environment Service, Downsview, Ontario (1984).

Cachorro, V. E., de Frutos, A. M., and Casanova, J. L., Determination of the Angström turbidity parameters, *Appl. Opt.* **26**, 3069–3076 (1987).

Davies, J. A., and Hay, J. E., Calculation of the solar radiation incident on a horizontal surface, *Proceedings 1st Canadian Solar Radiation Data Workshop*, AES, Toronto, 1978, pp. 32–58 (1980).

Dogniaux, R., Variations géographiques et climatiques des expositions énergétiques solaires sur des surfaces réceptrices horizontales et verticales, Tech. Rep. Misc. B38, Institut Royal Météorologique, Uccle, Belgium (1975).

Erbs, D. G., Klein, S. A., and Beckman, W. A. Estimation of degree-days and ambient temperature bin data from monthly-average temperatures, *ASHRAE J.*, **25**, 60–65 (1983).

Flowers, E. C., McCormick, R. A., and Kurfis, K. R., Atmospheric turbidity over the United States, *J. Appl. Meteorol.* **8**, 955–962 (1969).

Freund, J., Aerosol optical depth in the Canadian Arctic, *Atmosphere-Ocean*, **21**, 158–167 (1983).

Garrison, J. D., and Sahami, K., Analysis of clear sky solar radiation for seven Canadian sites, *Proc. SOLAR '93*, ASES, Washington, DC, pp. 445–450 (1993).

Garrison, J. D., and Adler, G. P., Estimation of precipitable water over the United States for application to the division of solar radiation into its direct and diffuse components, *Solar Energy*, **44**, 225–241 (1990).

Grenier, J. C., de la Casinière, A., and Cabot, T., A spectral model of Linke's turbidity factor and its experimental implications, *Solar Energy*, **52**, 303–313 (1994).

Gueymard, C., A two-band model for the calculation of clear sky solar irradiance, illuminance, and photosynthetically active radiation at the Earth's surface, *Solar Energy*, **43**, 253–265 (1989).

Gueymard, C., Assessment of the accuracy and computing speed of simplified saturation vapor equations using a new reference data set, *J. Appl. Meteorol.*, **32**, 1294–1300 (1993a).

Gueymard, C., Atmospheric turbidity in Florida, Prof. Paper No. 247, Florida Solar Energy Center, Cape Canaveral, FL (1993b).

Hay, J. E., Precipitable water over Canada. I—Computation, *Atmosphere*, **8**, 128–143 (1970).

Hay, J. E., Precipitable water over Canada: II—Distribution, *Atmosphere*, **9**, 101–111 (1971).

Hay, J. E., and Darby, R., El Chichon—Influence on aerosol optical depth and direct, diffuse and total solar irradiances at Vancouver, B. C., *Atmosphere-Ocean*, **22**, 354–368 (1984).

Iqbal, M., *An introduction to solar radiation*, Academic Press, Toronto (1983).

Latimer, J. R., Observation of direct solar radiation and atmospheric turbidity at Toronto-Scarborough from 1960 to 1970, Tech. Rep. CMRR 1/74, Atmospheric Environment Service, Downsview, Ontario (1974).

Leckner, B., The spectral distribution of solar radiation at the Earth's surface—elements of a model, *Solar Energy*, **29**, 143–150 (1978).

Lott, G. A., Precipitable water over the United States, Vol. 1: Monthly means, Tech. Rep. NWS 20, NOAA-NWS, Silver Spring, MD (1976).

Louche, A., Maurel, M., Simonnot, G., Peri, G., and Iqbal, M., Determination of Angström's turbidity coefficient from direct total solar irradiance measurements, *Solar Energy*, **38**, 89–98 (1987).

Michalsky, J. J., Perez, R., Seals, R., and Ineichen, P., Concentration system performance degradation in the aftermath of Mount Pinatubo, *Proc. Solar '93*, ASES, Washington, DC, pp. 495–500 (1993).

Myers, D. R., and Maxwell, E. L., Hourly estimates of precipitable water for solar radiation models, *Proc. Solar '92*, ASES, Cocoa Beach, FL, pp. 317–322 (1992).

Navvab, M., Karayel, M., Ne'eman, E., and Selkowitz, S., Analysis of atmospheric turbidity for daylight calculations, *Energy Build.*, **6**, 293–303 (1984).

NREL, *Interim solar radiation data manual*, Tech. Rep. NREL/TP-463-5176, National Renewable Energy Lab, Golden, CO (1992).

Peterson, J. T., and Flowers, E. C., Interactions between air pollution and solar radiation, *Solar Energy*, **19**, 23–32 (1977).

Polavarapu, R. J., Atmospheric turbidity over Canada, *J. Appl. Meteorol.*, **17**, 1368–1374 (1978).

Quinlan, F. T., (ed.), *Hourly solar radiation-surface meteorological observations, SOLMET, vol. 2*, Final Rep. TD-9724, National Climatic Center, Asheville, NC (1979).

Ratner, B., Upper-air climatology of the United States. Pt. 1—Averages for isobaric surfaces, Tech. Paper No. 32, U.S. Weather Bureau, Washington, DC (1957).

Reitan, C. H., Mean monthly values of precipitable water over the United States, 1946–56, *Mon. Weath. Rev.*, **88**, 25–35 (1960).

Reitan, C. H., Surface dew point and water vapor aloft, *J. Appl. Meteorol.*, **2**, 776–779 (1963).

Sadler, G. W., Turbidity of the atmosphere at solar noon for Edmonton, Alberta, Canada, *Solar Energy*, **21**, 339–342 (1978).

Schroeder, R., and Davies, J. A., Significance of nitrogen dioxide in estimating aerosol optical depth and size distributions, *Atmosphere-Ocean*, **25**, 107–114 (1987).

Shah, G. M., Aperture effects on atmospheric turbidity measurements, *Solar Energy*, **21**, 527–530 (1978).

Shands, A. L., Mean precipitable water in the United States, Tech. Paper No. 10, U.S. Weather Bureau, Washington, DC (1949).

Shaw, G. E., Error analysis of multi-wavelength sun photometry, *Pageoph*, **114**, 1–14 (1976a).

Shaw, G. E., Nitrogen dioxide—optical absorption in the visible, *J. Geophys. Res.*, **81**, 5791–5792 (1976b).

Simulation Research Group, *DOE-2 Supplement, version 2.1D*, Rep. LBL-8706, Rev. 5, Lawrence Berkeley Lab, Berkeley, CA (1989).

Titus, R. L., 1961–1970 Mean, extreme and standard deviation values for Canadian upper air stations, Rep. CLI-8-73, Atmospheric Environment Service, Downsview, Ontario (1973).

Uboegbulam, T. C., and Davies, J. A., Turbidity in eastern Canada, *J. Clim. Appl. Meteorol.*, **22**, 1384–1392 (1983).

Valko, P., Über den Zusammenhang zwischen Trübungsfaktor und Trübungs koeffizient, *Arch. Met. Geoph. Biokl.*, **B15**, 359–375 (1967).

Vignola, F., and McDaniels, D. K., Effects of El Chichon on global correlations, *Proceedings of the Conference of Intersol '85*, Pergamon Press, Montreal, pp. 2434–2438 (1986).

Winkelmann, F. C., Daylighting calculation in DOE-2, Rep. LBL-11353, Lawrence Berkeley Lab, Berkeley, CA (1983).

WMO, Atmospheric turbidity data for the world, WMO/EPA/NOAA (1971). The name of this yearly publication changed to *Atmospheric turbidity and chemistry data for the world* in 1972; to *Global monitoring of the environment for selected atmospheric constituents* in 1975; and to *Global atmospheric background monitoring for selected environmental parameters BAPMoN data* in 1978. Available from National Climatic Center, Asheville, NC, and World Meteorological Organization, Geneva, Switzerland.

Yamashita, S., A comparative study of turbidity in an urban and a rural environment at Toronto, *Atmos. Environ.*, **8**, 507–518 (1974).

Yue, G. K., McCormick, M. P., and Chiou, E. W., Stratospheric aerosol optical depth observed by the Stratospheric Aerosol and Gas Experiment II: Decay of the El Chichon and Ruiz volcanic perturbations, *J. Geophys. Res.*, **96D**, 5209–5219 (1991).